**GT2004-- 53965**

# A COMPREHENSIVE PROGNOSTICS APPROACH FOR PREDICTING
# GAS TURBINE ENGINE BEARING LIFE

**Rolf Orsagh, Michael Roemer, Jeremy Sheldon**
**Impact Technologies, LLC**
**125 Tech Park Drive**
**Rochester, NY 14623**
**585-424-1990**
**rolf.orsagh@impact-tek.com**

**Christopher J. Klenke**
**Air Force Research Lab.**
**1790 Loop Rd. North**
**Wright-Patterson AFB, OH 45433**

## ABSTRACT

Development of practical and verifiable prognostic approaches for gas turbine engine bearings will play a critical role in improving the reliability and availability of legacy and new acquisition aircraft engines. In addition, upgrading current United States Air Force (USAF) engine overhaul metrics based strictly on engine flight hours (EFH) and total accumulated cycles (TAC) with higher fidelity prognostic models will provide an opportunity to prevent failures in engines that operate under unusually harsh conditions, and will help avoid unnecessary maintenance on engines that operate under unusually mild conditions.

A comprehensive engine bearing prognostic approach is presented in this paper that utilizes available sensor information on-board the aircraft such as rotor speed, vibration, lube system information and aircraft maneuvers to calculate remaining useful life for the engine bearings. Linking this sensed data with fatigue-based damage accumulation models based on a stochastic version of the Yu-Harris bearing life equations with projected engine operation conditions is implemented to provide the remaining useful life assessment. The combination of health monitoring data and model-based techniques provides a unique and knowledge rich capability that can be utilized throughout the bearing's entire life, using model-based estimates when no diagnostic indicators are present and using the monitored features such as oil debris and vibration at later stages when failure indications are detectable, thus reducing the uncertainty in model-based predictions. A description and initial implementation of this bearing prognostic approach is illustrated herein, using bearing test stand run-to-failure data and engine test cell data.

## INTRODUCTION

A comprehensive prognostic capability can be achieved for rolling element bearings through the integration of health state awareness with model-based damage assessments. The basis for this prediction is an intelligent fusion of diagnostic features and physics-based modeling. Since bearings have many failure modes and there are many influencing factors, a modular approach is taken in the design.

As stated above there are many potential failure modes for rolling element bearings and to completely discuss all modes is beyond the scope of this paper. Therefore only the normal rolling contact fatigue failure mode, herein called spalling, is discussed. Also other failure modes may cause conditions that result in spalling (3). For instance Brinnell marks can cause localized stress concentrations that prematurely cause spalling.

Some failure modes are not applicable to the prognostic architecture. Maintenance induced failures (misalignment, incorrect installation, etc.) are impossible to predict. Contamination of the lubricant is one of the most common failure modes, but it is impossible to predict when the lubricant will become contaminated. However, it is possible to detect the conditions, through sensor information, that precede these failures and adjust the prediction accordingly, such as detection of water in the lubricant would reduce the fatigue life prediction.

Assessment of remaining life entails three functional steps as shown in Figure 1: Sensed Data, Current Bearing Health, and Future Bearing Health. The RUL prediction process begins with the Sensed Data module. Signals indicative of bearing health (vibration, oil debris, temperature, etc) are monitored to determine the current bearing condition. Diagnostic features extracted from these signals are then passed on to Current Bearing Health module. These diagnostic features are low-level signal extraction type features, such as root mean square (RMS), kurtosis, and high frequency enveloped features. In addition engine speed and maneuver induced loading are outputted for use as inputs to bearing health models. Also extracted are characteristic features that can be used to identify failure of a particular bearing component (ball, cage, inner or outer raceway).

| | | Form Approved OMB No. 0704-0188 |
|---|---|---|

# Report Documentation Page

*Form Approved*
*OMB No. 0704-0188*

Public reporting burden for the collection of information is estimated to average 1 hour per response, including the time for reviewing instructions, searching existing data sources, gathering and maintaining the data needed, and completing and reviewing the collection of information. Send comments regarding this burden estimate or any other aspect of this collection of information, including suggestions for reducing this burden, to Washington Headquarters Services, Directorate for Information Operations and Reports, 1215 Jefferson Davis Highway, Suite 1204, Arlington VA 22202-4302. Respondents should be aware that notwithstanding any other provision of law, no person shall be subject to a penalty for failing to comply with a collection of information if it does not display a currently valid OMB control number.

| 1. REPORT DATE **JUN 2004** | 2. REPORT TYPE | 3. DATES COVERED **00-00-2004 to 00-00-2004** |
|---|---|---|
| 4. TITLE AND SUBTITLE **A Comprehensive Prognostics Approach for Predicting Gas Turbine Engine Bearing Life** | | 5a. CONTRACT NUMBER |
| | | 5b. GRANT NUMBER |
| | | 5c. PROGRAM ELEMENT NUMBER |
| 6. AUTHOR(S) | | 5d. PROJECT NUMBER |
| | | 5e. TASK NUMBER |
| | | 5f. WORK UNIT NUMBER |
| 7. PERFORMING ORGANIZATION NAME(S) AND ADDRESS(ES) **Impact Technologies LLC,200 Canal View Blvd,Rochester,NY,14618** | | 8. PERFORMING ORGANIZATION REPORT NUMBER |
| 9. SPONSORING/MONITORING AGENCY NAME(S) AND ADDRESS(ES) | | 10. SPONSOR/MONITOR'S ACRONYM(S) |
| | | 11. SPONSOR/MONITOR'S REPORT NUMBER(S) |
| 12. DISTRIBUTION/AVAILABILITY STATEMENT **Approved for public release; distribution unlimited** | | |
| 13. SUPPLEMENTARY NOTES **Proceedings of IGTI TurboExpo 2004 Vienna, June 14-17, 2004** | | |
| 14. ABSTRACT **see report** | | |
| 15. SUBJECT TERMS | | |

| 16. SECURITY CLASSIFICATION OF: | | | 17. LIMITATION OF ABSTRACT | 18. NUMBER OF PAGES | 19a. NAME OF RESPONSIBLE PERSON |
|---|---|---|---|---|---|
| a. REPORT **unclassified** | b. ABSTRACT **unclassified** | c. THIS PAGE **unclassified** | **Same as Report (SAR)** | **9** | |

**Standard Form 298 (Rev. 8-98)**
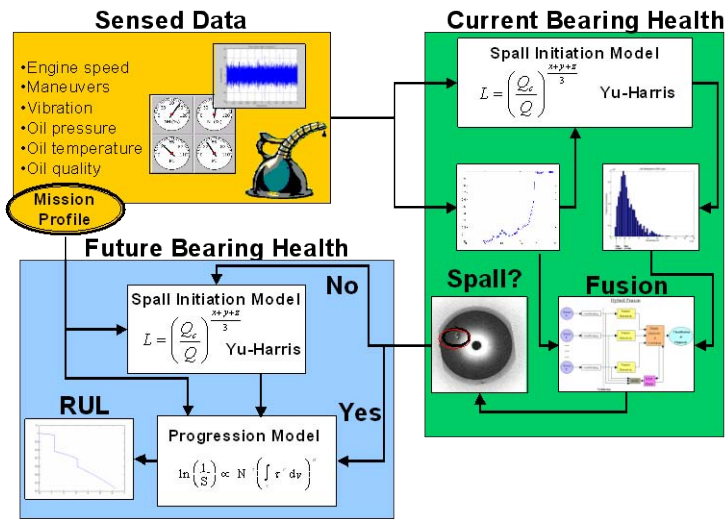Prescribed by ANSI Std Z39-18

**Figure 1** Overall Prognostic Architecture

Central to the next step is a rolling contact fatigue (RCF) model. This model utilizes information from the Sensed Data module to calculate the cumulative damage sustained by the bearing since it was first installed. Life limiting parameters used by the RCF model such as load, and lubricant film thickness are derived from the sensed data using physics-based and empirical models. Utilizing knowledge fusion this probability is combined with the extracted features that are indicative of spalling. Combining the model output with the features improves the robustness and accuracy of the prediction.

Whether or not a spall exists determines the next step. If a spall does not currently exist the spall initiation prognostic module is used to forecast the time to spall initiation. This forecast is based on the same model that is used to assess the current probability of spall initiation, but instead the model uses projected future operating conditions (loads, speeds, etc.) rather than the current conditions. Then the initiation results are passed to the progression model, which also uses the mission profile to allow an accurate prediction on the time from spall initiation to failure. If a spall currently exists the initiation prognostic module is bypassed and the process described above is performed directly.

## VIBRATION BASED FEATURES

Development of the vibration features is a critical step in the design of the integrated system mentioned above. To this end, a series of tests was conducted to provide data for algorithm testing. Vibration and oil debris data acquired from a ball bearing test rig in with a damaged bearing was installed is used to compare the effectiveness of various diagnostic features. Vibration data acquired from a gas turbine engine running in a test cell provides more realistic data that includes multiple excitation sources and background noise. Distinguishing bearing signatures from the background noise of an operating engine presents a significant technical challenge. To test the ability of vibration analysis algorithms to observe weak bearing signatures, the bearings in the engine did not contain any known faults.

For the faulted bearing tests, data was collected from a miniaturized lubrication system simulator, called the Minisimulator, located at the Air Force Research Laboratory (ARFL) on Wright Patterson Air Force Base (3). This data was collected with much support from the University of Dayton Research Institute (UDRI) and the AFRL. The Minisimulator consists of a test head as shown in Figure 2 and a lubrication sump. A pair of angular contact bearings located in the test head support a rotating shaft. The bearings are identical to the number 2 main shaft bearing of an Allison T63 gas turbine engine.
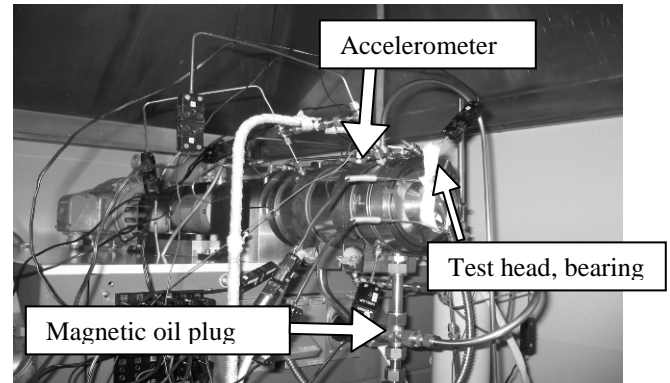


**Figure 2**-Minisimulator Setup

Although designed primarily for lubrication tests, the Minisimulator was used to generate accelerated bearing failures. One run-to-failure seeded fault test was run. To accelerate the bearing failure, a fault was seeded into the inner raceway of one of the bearings by means of a small hardness indentation (Brinnell mark). The bearing was then loaded to approximately 14,234 N (3200 lbf) and ran at a constant speed of 12000 RPM (200 Hz). Vibration data was collected from a cyanoacrylate–mounted (common called Super Glue) accelerometer, which was sampled at over 200 kHz. Also, the quantity of debris in the oil draining from the test head was measured using a magnetic chip collector (manufactured by Eateon Tedeco). The oil data was used in determining the initiation of the spall.

For the engine tests, data was collected from a T63 engine located in a test cell, also at AFRL. The T63 tests were performed at two gas generator speed levels, a "cruise speed" of 50,000 RPM (833 Hz) and an "idle speed" of 32,000 RPM (533 Hz). Dimensions of the bearings of interest are given in Table 1.

**Table 1**-Bearing Dimensions (mm)

| Bearing | Ball Diameter (Bd) | Number of balls (z) | Pitch Diameter (Pd) | Contact Angle (β) |
|---------|--------------------|--------------------|--------------------|--------------------|
| # 1 | 4.7625 | 8 | 42.0624 | 18.5° |
| # 2 | 7.9375 | 13 | 42.0624 | 18.5° |

## FAULT FREQUENCIES

The fundamental pass frequencies of the components of a bearing can be easily calculated with equations from reference

(4). Extraction of the vibration amplitude at these frequencies from a fast Fourier Transform (FFT) often enables isolation of the fault to a specific bearing in an engine. High amplitude of vibration at any of these frequencies indicates a fault in the associated component.

Table 2 is the calculated minisimulator bearing fault frequencies. Table 3 and Table 4 summarize the two bearings of interest for the T63 engine.

**Table 2**-Minisimulator Bearing Fault Frequencies (Hz)

| Shaft Speed | BSF | BPFI | BPFO | Cage |
|---|---|---|---|---|
| 200 | 512 | 1530 | 1065 | 82 |

**Table 3**-T63 #1 Bearing Fault Frequencies (Hz)

| Shaft Speed | BSF | BPFI | BPFO | Cage |
|---|---|---|---|---|
| 533 | 2327 | 2361 | 1931 | 238 |
| 833 | 3636 | 3690 | 2974 | 372 |

**Table 4-**T63 #2 Bearing Fault Frequencies (Hz)

| Shaft Speed | BSF | BPFI | BPFO | Cage |
|---|---|---|---|---|
| 533 | 1367 | 4085 | 2845 | 219 |
| 833 | 2136 | 6384 | 4456 | 342 |

Note the listings are defined by:

BSF: Ball Spin Frequency
BPFI: Inner Raceway Frequency
BPFO: Outer Raceway Frequency
Cage: Cage Frequency

Periodic forces associated with meshing of gear teeth also excite vibration at specific frequencies. These gear mesh frequencies (GMF) are calculated for several of the gears in the T-63 engine ands summarized in Table 5. The calculated GMFs for the T-63 gas producer and power turbine gear trains are for an idle speed of 32,000 RPM. The speed ratio (the ratio of the gear speed to the gas producer (GP) input gear speed) may be used to calculate the gear mesh frequencies at other gas producer speeds.

**Table 5**-T-63 Gear Mesh Frequencies (Hz)

| Gear | Speed Ratio (to GP shaft speed) | GMF @ 533 Hz |
|---|---|---|
| A | 1 .000 | 9061 |
| B | 0.202 | 3775 |
| C | 0.202 | 9061 |
| D | 0.08 | 3775 |
| E | 0.151 | 3777 |
| F | 0.236 | 3775 |
| G | 0.252 | 1125 |
| H | 0.073 | 1124 |
| I | 0.117 | 3128 |
| J | 0.117 | 2315 |
| K | 0.099 | 2315 |
| L | 0.082 | 2315 |
| M | 0.196 | 8758 |

## HIGH FREQUENCY ENVELOPING

Although bearing characteristic frequencies are easily calculated, they are not always easily detected by conventional frequency domain analysis techniques. Vibration amplitudes at these frequencies due to incipient faults (and sometimes more developed faults) are often indistinguishable from background noise or obscured by much higher amplitude vibration from other sources including engine rotors, blade passing, and gear mesh in a running engine. However, bearing faults produce impulsive forces that excite vibration at frequencies well above the background noise in an engine.

Impact Energy™ is an enveloping-based vibration feature extraction technique (5). The enveloping process consists of first band pass filtering of the raw vibration signal. Second, the band pass filtered signal is full waved rectified to extract the envelope. Third, the rectified signal is passed through a low pass filter to remove the high frequency carrier signal. Finally, the signal has any DC content removed.

The Impact Energy™ was applied to the seeded fault test data collected using the Minisimulator. To provide the clearest identification of the fault frequencies, several band pass and low pass filters were used of analyze various regions of the vibration spectrum. Using multiple filters allowed investigation of many possible resonance's of the bearing test rig and its components. A sample Impact Energy™ spectrum from early in the Minisimulator test is shown in Figure 3. Note that this data was collected prior to spall initiation (based on oil debris data), and the feature response is due the indentation on the race.

For comparison, a conventional FFT (10 frequency domain averages) of vibration data was also calculated and is shown in Figure 4. In the conventional frequency domain plot (Figure 4) there is no peak at the inner race ball pass frequency (1530 Hz). However, the Impact Energy™ plot (Figure 3) shows clearly defined peaks at this frequency and the second through forth harmonics of the inner race ball pass frequency. These peaks were defined using a detection window of ± 5 Hz about the theoretical frequency of interest to account for bearing slippage. From the onset of the test there is an indication of a fault.
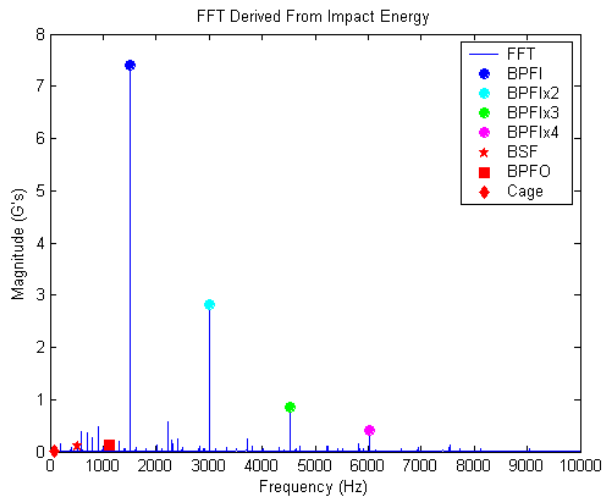
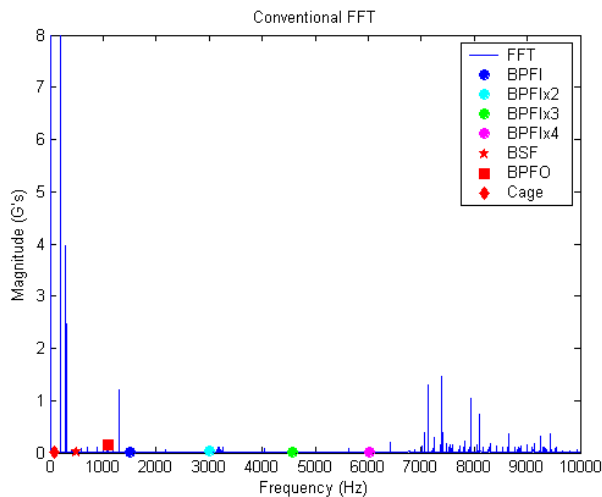**Figure 3**-Impact Energy™ FFT of Minisimulator-Seeded Fault



**Figure 5**-Impact Energy™ FFT of Minisimulator-No Fault



**Figure 4**-Conventional FFT of Minisimulator-Seeded Fault
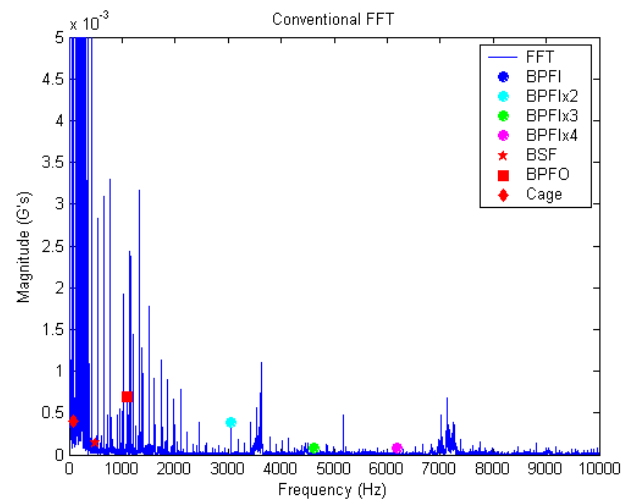


**Figure 6**-Conventional FFT of Minisimulator-No Fault

Previous minisimulator tests were conducted on un-faulted "healthy" bearings. Although these were run-to-failure tests there was no seeding of a fault. Below are two plots for comparison with the seeded fault test. Figure 5 shows the Impact Energy™ derived FFT from the minisimulator test with the un-faulted bearing. Notice the much lower magnitude for this plot and Figure 6, which is the conventional FFT. Although the high magnitude of at the BPFI in Figure 5 appears to indicate a fault it merely is an indication of possible bearing flaws.

Data from the T63 engine (running at the idle shaft speed of 32,000 RPM) was also analyzed using both conventional frequency domain analysis and Impact Energy™. This data presents a greater challenge to the analysis techniques for two reasons: First, the bearings in the engine do not contain any known faults. Second, the bearing signatures may be obscured by much higher amplitude vibration from random noise and other sources of vibration energy including blade passing, and gear mesh in the engine.

Identification of vibration features in a running engine is very difficult due to the high ambient noise level, which often obscures diagnostic features. Despite the fact that the bearings and gears in the engine are healthy, minor imperfections within manufacturing tolerances cause slightly elevated vibration levels at the characteristic frequencies. Raceway and ball waviness, surface finish imperfections and dimensional tolerances can lead to vibration signatures in a healthy engine (4). Vibration analysis techniques that are able to distinguish these signatures from a healthy bearing in running engine are

4

considered the most likely to detect the signature of a defective bearing, because they are more sensitive than other techniques.

Figure 7 shows a conventional frequency domain analysis of the T63 engine data with the locations of the bearing characteristic frequencies identified. However, the vibration amplitudes at these frequencies cannot be distinguished from the noise floor.
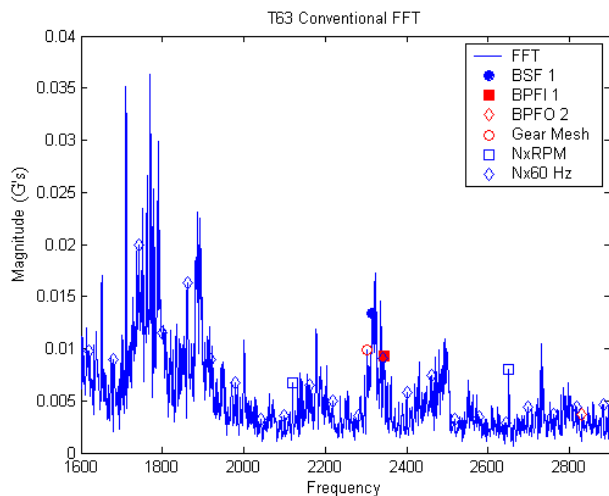


**Figure 7**-T63 Conventional FFT

The most prominent features in the Impact Energy™ spectrum in Figure 8 are harmonics of the gas generator shaft speed (NxRPM). Although less prominent, a gear mesh frequency (GMF) and the outer race characteristic frequency of the number 2 bearing (BPFO 2) are also observable. Low amplitude vibration at a gear mesh frequency does not necessarily indicate that a problem exists. The low amplitude vibration at a characteristic bearing frequency may be attributable to a benign bearing condition as well. However, observation of these features illustrates the ability of Impact Energy to detect incipient faults.

Although most of the peaks have been identified several still are unidentified. In a turbine engine there are many gears and even more bearings, which have distinct frequencies. In addition there are frequencies associated with the compressor and turbine blades.
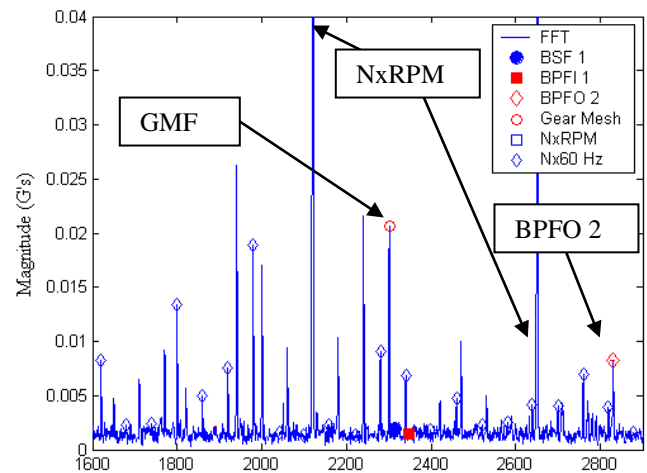


**Figure 8**-T63 Impact Energy™ FFT, Showing Frequencies at Calculated Frequencies but Found Magnitudes

In addition to the above features conventional vibration features are used. Although traditional statistical based such as RMS, kurtosis, crest value, and peak value are valuable to the prognostics they are not represented (9). These other features are used in combination with Impact Energy™, to avoid false alarms.

## FUSION OF MODEL AND SENSOR-BASED INFORMATION

Model and sensor-based diagnostic approaches offer complementary condition assessment information that can be fused to achieve a comprehensive diagnostic/prognostic capability throughout a components life. Model-based approaches provide valuable damage accumulation information on critical components well in advance of failure indications. Due to modeling uncertainties, these long-range predictions typically have broad confidence bounds. Sensor-based approaches provide direct measures of component condition that can be used to update the modeling assumptions and reduce the uncertainty in the RUL predictions.

To achieve a comprehensive diagnostic/prognostic capability throughout the life of critical engine components, model-based information is used to predict the initiation of a fault. In most cases, these predictions will prompt "just in time" maintenance actions to prevent the fault form developing. However, due modeling uncertainties, incipient faults may occasionally develop earlier than predicted. In these situations, sensor-based diagnostics complement the model-based prediction by updating the model to reflect the fact that fault initiation has occurred. Subsequent predictions of the remaining useful component life will be based on fault progression rather than initiation models.

*Spall Initiation Model*
A variety of theories exist for predicting spall initiation from bearing dimensions, loads, lubricant quality, and a few empirical constants. Many modern theories are based on the Lundberg-Palmgren (L-P) model that was developed in the

1940's (1). A model proposed by Ioannides and Harris (I-H) improved on the L-P model by accounting for the evidence of fatigue limits for bearings (6). Yu and Harris (Y-H) proposed a stress-based theory in which relatively simple equations are used to determine the fatigue life purely from the induced stress (7). This approach depends to lesser extent on empirical constants, and the remaining constants may be obtained from elemental testing rather than complete bearing testing as required by L-P.

The fundamental equation of the Y-H model stated in equation 1 relates the survival rate (S) of the bearing to a stress weighted volume integral as shown below. The model utilizes a new material property for the stress exponent (c) to represent the material fatigue strength, and the conventional Weibull slope parameter to account for dispersion in the number of cycles (N). The fatigue initiating stress ($\tau$) may be expressed using Sines multi-axial fatigue criterion for combined alternating and mean stresses, or as a simple Hertz stress (8).

**Error! Objects cannot be created from editing field codes.** (1)

For simple Hertz stress, a power law is used to express the stress-weighted volume. In equation 2 below, $\lambda$ is the circumference of the contact surface, and a and b are the major and minor axes of the contact surface ellipse. The exponent values were determined by Yu and Harris for b/a $\approx$ 0.1 to be x=0.65, y=0.65, and z=10.61. Yu and Harris assume that these values are independent of the bearing material.

**Error! Objects cannot be created from editing field codes.** (2)

According to the Y-H model, the life ($L_{10}$) of a bearing is a function of the basic dynamic capacity ($Q_c$) and the applied load as stated below in equation 3. Where, the basic dynamic capacity is given in equation 4. A lubrication effect factor may be introduced to account for variations in film thickness due to temperature, viscosity, and pressure. Although this approach was developed for angular contact ball bearings, it is extendable to other bearing types such as tapered roller and cylindrical bearings.

**Error! Objects cannot be created from editing field codes.** (3)

**Error! Objects cannot be created from editing field codes.** (4)

**Error! Objects cannot be created from editing field codes.** (5)

Where:

$A_1$ = Material property
T = A function of the contact surface dimensions
$T_1$ = value of T when a/b = 1
u = number of stress cycles per revolution
D = Ball diameter

$\rho$ = Curvature (inverse radii of component)
d = Component (race way) diameter
a* = Function of contact ellipse dimensions
b* = Function of contact ellipse dimensions

## MODEL VALIDATION

Validation of the spall initiation model requires a comparison of actual fatigue life values to predicted model values. Acquiring sufficient numbers of actual values is not a trivial task. Under normal conditions it is not uncommon for a bearing life value to extend past 100 million cycles, prohibiting normal run-to-failure testing.

Accelerated life testing is one method used to rapidly generate many bearing failures. By subjecting a bearing to high speed, load, and/or temperature, rapid failure can be induced. There are many test apparatus used for accelerated life testing including ball and rod type test rigs. One such test rig is operated by UES, Inc at the Air Force Research Laboratory (AFRL) at Wright Patterson Air Force Base in Dayton, OH. A simple schematic of the device is shown in Figure 9 with dimensions given in millimeters. This rig consists of three 12.7 mm diameter balls contacting a 9.5 mm rotating central rod see Table 6 for dimensions. The three radially loaded balls are pressed against the central rotating rod by two tapered bearing races that are thrust loaded by three compressive springs. A photo of the test rig is shown in Figure 10. Notice the accelerometers mounted on the top of the unit. The larger accelerometer is used to automatically shutdown the test when a threshold vibration level is reached, the other measures vibration data for analysis.
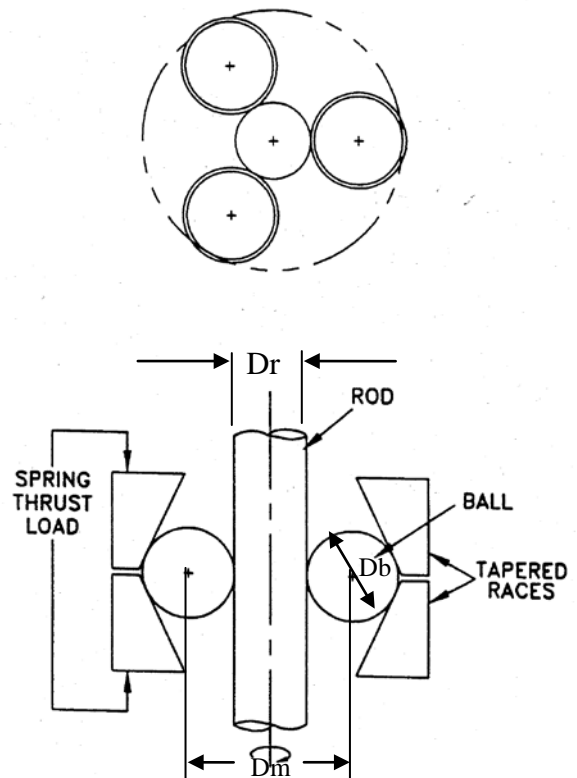
Figure 9 Schematic of Rolling Contact Fatigue Tester

**Table 6**- Rolling Contact Fatigue Tester Dimensions (mm)

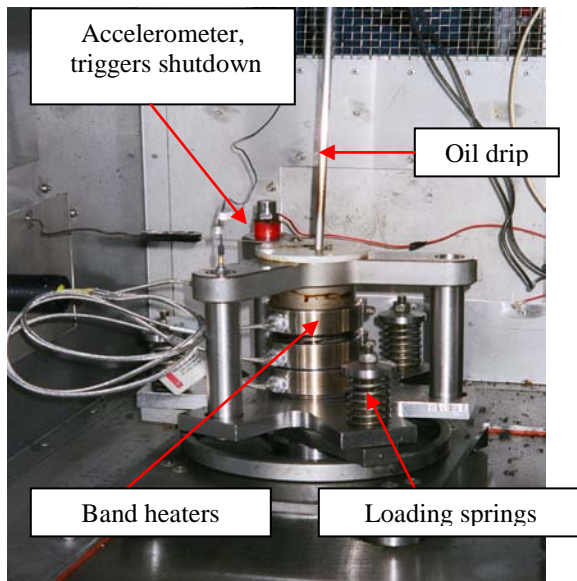| Rod diameter (Dr) | 9.52 |
|---|---|
| Ball diameter (Db) | 12.70 |
| Pitch diameter (Dm) | 22.23 |



**Figure 10**-Rolling Contact Fatigue Tester

By design the rod is subjected to high contact stresses. Due to the geometry of the test device, the 222 N (50 lbs) load applied by the springs translates to a 942 N (211 lbs) load per ball on the center rod. Assuming Hertzian contact for balls and rod made of M50 bearing steel, the 942 N radial load results in a maximum stress of approximately 4.8 GPa (696 ksi). This extremely high stress causes rapid fatigue of the bearing components and can initiate a spall in less than 100 hours, depending on test conditions including lubrication, temperature, etc. Since failures occur relatively quickly, it is possible to generate statistically significant numbers of events in a timely manner.

For validation purposes M50 rods and balls were tested at room temperature (23°C). The results of these tests are in Table 7. A summary plot is shown in Figure 11.

**Table 7** RCF Fatigue Life Results

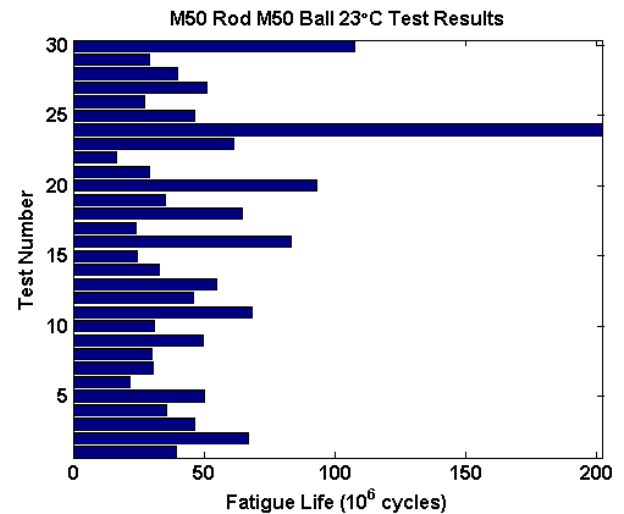| Failures (#) | Susp (#) | Susp Time (cylces) |
|---|---|---|
| 29 | 1 (ball failed) | 83.33 |



**Figure 11** RCF Fatigue Life Results

*Stochastic Model*

As stated above one of the issues with empirical/physics based models is their inherent uncertainty. Assumptions and simplifications are made in all modeling and not all of the model variables are exactly known. Often stochastic techniques are used to account for the implicit uncertainty in a model's results. Statistical methods are used to generate numerous possible values for each input.

A Monte Carlo simulation was utilized in the calculation of the bearing life distribution. Inputs to the model were represented by normal or lognormal distributions to approximate the uncertainty of the input values. Sample input distributions to the model are shown in Figure 12.
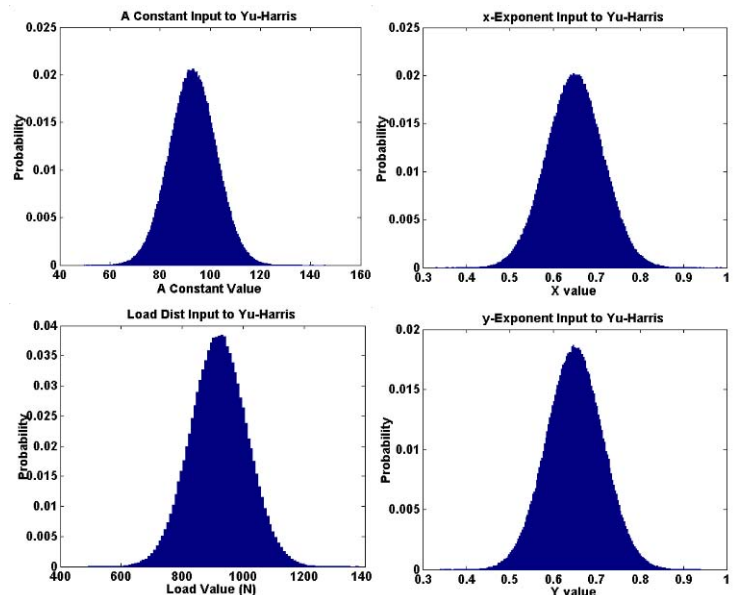


**Figure 12**-Model Input Distributions

## Comparison

The Yu-Harris model was used to simulate the room temperature M50 RCF tests. Figure 13 shows the results for a series of the room temperature RCF tests on the M50 bearing material. This test was run at 3600 RPM at room temperature with the 7808K lubricant. The y-axis is the number of central rod failures and the x-axis is the millions of cycles to failure.

The predicted life from the model is shown in Figure 13 also, superimposed on the actual test results. This predicted distribution shown in red was calculated from the model using one million Monte Carlo points.
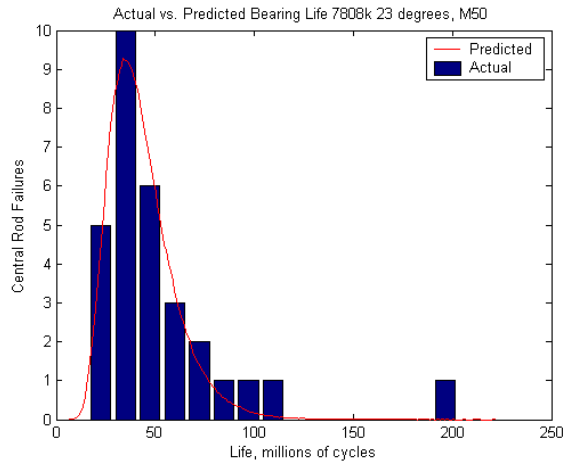


**Figure 13**-Room Temp Results vs. Predicted

In Figure 14, the median ranks of the actual lives (blue dots) are plotted against the cumulative distribution function (CDF) of the predicted lives (blue line). The model predicted lives are slightly more conservative (in the sense that the predicted life is shorter than the observed life) once the cumulative probability of failure exceeds 70%. However since bearings are a critical component, the main interest is in the left most region of the distribution where the first failures occur and
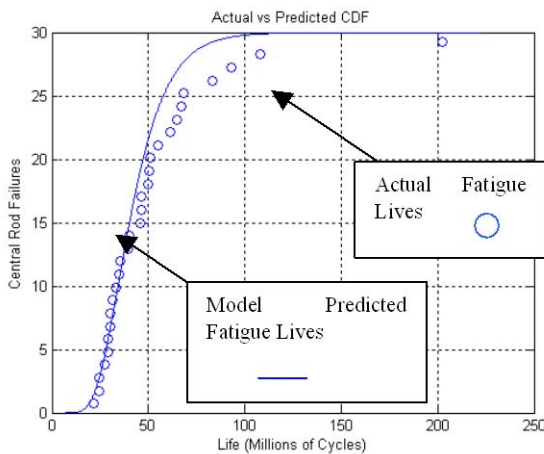


the model correlates better.

**Figure 14**-Actual Life vs. Predicted Life

Calculation of median ranks is a standard statistical procedure for plotting failure data. During run-to-failure testing there are often tests that either are prematurely stopped before failure or a failure occurs of a component other than the test specimen. Although the data generated during these failures are the mode of interest, they provide a lower bound on the fatigue lives due to the failure mode of interest. One method for including this data is by median ranking.

The median rank was determined using Benard's Median Ranking method, which is stated in equation 6 below. This method accounts for tests that did not end in the failure mode of interest (suspensions). In the case of the ball and rod RCF test rig, the failure mode of interest is creation of a spall on the inner rod. The time to suspension provides a lower bound for the life of the test article (under the failure mode of interest), which can be used in reliability calculations. During the testing on the RCF test rig, significant portions of the tests were terminated without failure after reaching ten times the $L_{10}$ life. There were also several tests that ended due to development of a spall on one of the balls rather than on the central rod.

$$\text{Benard's Median Rank} = \frac{(\text{AR} - 0.3)}{(\text{N} + 0.4)} \qquad (6)$$

Where:

$$\text{AR} = \text{Adjusted Rank}$$

$$\text{N} = \text{Number of Suspensions and Failures}$$

The adjusted rank is calculated below.

$$\text{AR} = \frac{(\text{Reverse Rank})x(\text{Previous Adjusted Rank}) + (\text{N} + 1)}{\text{Reverse Rank} + 1}$$

(7)

Although the test does not simulate an actual bearing assembly in an engine, it does simulate similar conditions (1). Materials and the geometry of the bearing and the lubricants are the same for the test rig as they are in the T-63 engine. The test rig results validate the model's ability to predict the fatigue life of the material under similar conditions to an operating engine.

## CONCLUSION

To achieve a comprehensive diagnostic/prognostic capability throughout the life of critical engine components, model-based information is used to predict the initiation of a fault. In most cases, these predictions will prompt "just in time" maintenance actions to prevent the fault form developing. However, due modeling uncertainties, incipient faults may occasionally develop earlier than predicted. In these situations, sensor-based diagnostics complement the model-based prediction by updating the model to reflect the fact that fault initiation has occurred. Sensor-based approaches provide direct measures of component condition that can be used to update the modeling assumptions and reduce the uncertainty in the RUL predictions. Subsequent predictions of the remaining useful component life will be based on fault progression rather than initiation models.

Real-time algorithms for predicting and detecting bearing and gear failures are currently being developed in parallel with emerging flight-capable sensor technologies including in-line oil debris/condition monitors, and vibration analysis MEMS. These advanced prognostic/diagnostic algorithms utilize intelligent data fusion architectures to optimally combine sensor data, with probabilistic component models to achieve the best decisions on the overall health of oil-wetted components. By utilizing a combination of health monitoring data and model-based techniques, a comprehensive component prognostic capability can be achieved throughout a components life, using model-based estimates when no diagnostic indicators are present and monitored features such as oil debris and vibration at later stages when failure indications are detectable.

## REFERENCES

1. Toth, Douglas K., Saba, Costandy S., Klenke, Christopher J. "Minisimulator for Evaluating High-Temperature Canidate Lubricants Part I- Method Development," University Dayton Research Institute-Aero Propulsion Directorate USAF, Dayton, OH, 2001.

2. Glover, Douglas. "A Ball-Rod Rolling Contact Fatigue Tester," *Rolling Contact Fatigue Testing of Bearing Steels, ASTM STP 771*, ASTM, 1982, pp. 107-125.

3. Harris, T. (4th Edition 2001), *Rolling Bearing Analysis*, John Wiley & Sons, New York.

4. Wensig, J. A.," On the Dynamics of Ball Bearings," PhD Thesis, University of Twente, The Netherlands, pp 90, 1998.

5. Orsagh, Rolf F., Sheldon, Jeremy, Klenke, Christopher J., "Prognostics/Diagnostics for Gas Turbine Engine Bearings," *Presented at STLE Annual Meeting 2003*, STLE, NY, NY, publication pending.

6. Ioannides, and Harris, "A New Fatigue Life Model for Rolling Bearings", Journal of Tribology, Vol. 107, pp. 367-378, 1985

7. Yu, and Harris, "A New Stress-Based Fatigue Life Model for Ball Bearings", Tribology Transactions, Vol. 44, pp. 11-18, 2001

8. Sines, and Ohgi, "Fatigue Criteria Under Combined Stresses or Strains", ASME Journal of Eng. Materials and Tech., Vol. 103, pp. 82-90, 1981

9. Abernethy, Robert B., "The New Weibull Handbook," 1998.